# Electron Transfer from Flavin to Iron in the *Pseudomonas oleovorans* Rubredoxin Reductase−Rubredoxin Electron Transfer Complex†

Ho Joon Lee, Jaswir Basran, and Nigel S. Scrutton*

*Department of Biochemistry, University of Leicester, University Road, Leicester LE1 7RH U.K.*

*Received August 3, 1998; Revised Manuscript Received September 9, 1998*

ABSTRACT: Rubredoxin reductase (RR) and rubredoxin form a soluble and physiological eT complex. The complex provides reducing equivalents for a membrane-bound $\omega$-hydroxylase, required for the hydroxylation of alkanes and related compounds. The gene (*alk*T) encoding RR has been overexpressed and the enzyme purified in amounts suitable for studies of eT by stopped-flow spectroscopy. The eT reactions from NADH to the flavin of RR and from reduced RR to the 1Fe and 2Fe forms of rubredoxin have been characterized by transient kinetic and thermodynamic analysis. The reductive half-reaction proceeds in a one-step reaction involving oxidized enzyme and a two-electron-reduced enzyme−$NAD^+$ charge-transfer complex. Flavin reduction is observed at 450 nm and charge-transfer formation at 750 nm; both steps are hyperbolically dependent on NADH concentration. The limiting flavin reduction rate ($180 \pm 4\ s^{-1}$) is comparable to the limiting rate for charge-transfer formation ($189 \pm 7\ s^{-1}$) and analysis at 450 and 750 nm yielded enzyme−NADH dissociation constants of $36 \pm 2$ and $43 \pm 5\ \mu M$, respectively. Thermodynamic analysis of the reductive half-reaction yielded values for changes in entropy ($\Delta S^{\ddagger} = -65.8 \pm 2.2$ J $mol^{-1}$ $K^{-1}$), enthalpy ($\Delta H^{\ddagger} = 37.8 \pm 0.6$ kJ $mol^{-1}$) and Gibbs free energy ($\Delta G^{\ddagger} = 57.5 \pm 0.7$ kJ $mol^{-1}$ at 298 K) during hydride ion transfer to the flavin N5 atom. Spectral analysis of mixtures of 1Fe or 2Fe rubredoxin and RR suggest that conformational changes accompany eT complex assembly. Both the 1Fe (nonphysiological) and 2Fe (physiological) forms of rubredoxin were found to oxidize two electron-reduced rubredoxin reductase with approximately equal facility. Rates for the reduction of rubredoxin are hyperbolically dependent on rubredoxin concentration and the limiting rates are $72.7 \pm 0.6$ and $55.2 \pm 0.3\ s^{-1}$ for the 1Fe and 2Fe forms, respectively. Analysis of the temperature dependence of eT to rubredoxin using eT theory revealed that the reaction is not adequately described as a nonadiabatic eT reaction ($H_{AB} \gg 80\ cm^{-1}$). eT to both the 1Fe and 2Fe forms of rubredoxin is therefore gated by an adiabatic process that precedes the eT reaction from flavin to iron. Possible origins of this adiabatic event are discussed.

The mechanisms of eT[1] between soluble and physiological redox proteins have been the focus of recent and intensive investigation (e.g., refs *1*−*6*). The coexistence of protein−protein complexes in dissociative equilibrium with their constitutive reactants is a general feature of these reactions. The weak association of the constitutive proteins provides additional complexity in the control of interprotein eT rates compared with those eT reactions that occur within a single protein molecule. Whereas the specific interactions involved in the formation of tightly bound protein complexes can be elucidated by high-resolution structural methods—for example, NMR and X-ray crystallography—those responsible for the weaker eT complexes are poorly understood. This results from the inability of current structural methods to accommodate the lability of the weaker protein−protein complexes—although there are notable exceptions (*7*, *8*). In many cases, the components of eT complexes are thought to associate in suboptimal configurations via nonspecific interactions and then undergo a diffusional search for the specific optimal orientation commensurate with eT—the so-called reduction-in-dimensionality principle (*9*). Configurational gating (*10*) and gating of eT by proton transfer (*11*) or metal ions (*12*) has been demonstrated. In at least one case, a large-scale structural reorganization is thought to accompany complex formation (*13*), although in this latter system observed transfer rates measured by stopped-flow spectroscopy were shown to be intrinsic eT rates (*1*). Conformationally coupled transfer—in which a rapid but unfavorable step precedes eT—has been demonstrated for eT between methanol dehydrogenase and cytochrome *c*-551i (*5*). Control of interprotein eT is therefore not restricted to the physical parameters that control the *intrinsic* rate of eT—i.e., thermodynamic driving force, reorganizational energy, electronic coupling matrix element, and eT distance (*14*), since preceding adiabatic events may wholly or partially limit the transfer process (*15*). Studies of eT in physiological complexes will therefore provide more detailed insight into these adiabatic processes and their importance in controlling interprotein eT reactions.

The rubredoxin reductase (RR)−rubredoxin eT complex of *Pseudomonas oleovorans* is a physiological system that

† This work was funded by the Royal Society and the U.K. Biotechnology and Biological Sciences Research Council.

* Author to whom correspondence should be addressed. Tel: +44 116 233 1337. Fax: +44 116 252 3369. E-mail: nss4@le.ac.uk.

[1] Abbreviations: RR, rubredoxin reductase; eT, electron transfer.

10.1021/bi981853v CCC: $15.00 
Published on Web 10/16/1998

lends itself to studies of interprotein eT. These two soluble proteins, together with a membrane bound $\omega$-hydroxylase, are responsible for the hydroxylation of aliphatic hydrocarbons, functionalized hydrocarbons, and various aromatic compounds (*16*−*19*):

$$R{-}CH_3 + NADH + H^+ + O_2 \rightarrow R{-}CH_2OH + NAD^+ + H_2O$$

The hydroxylase component is a member of the nonhaem diiron family of proteins (*20*) that includes toluene-4-monooxygenase (*21*), methane monooxygenase (*22*), stearoyl-acyl carrier protein $\Delta^9$desaturase (*23*), rubrerythrin (*24*), and ribonucleotide reductase (*25*). RR is an NADH-dependent flavoprotein that transfers electrons from reduced nicotinamide to rubredoxin (*17*). The rubredoxin component is unique in possessing two Fe-binding domains (*18*) that have probably arisen by a process of gene duplication (*26*). The function of rubredoxin is to transfer reducing equivalents from RR to the membrane-bound $\omega$-hydroxylase (*27*). In recent years, the $\omega$-hydroxylase eT chain has been the focus of extensive genetic and biotechnological investigation, but corresponding structural and kinetic studies are lacking. With these deficiencies in mind, we recently reported the expression and purification of *Ps. oleovorans* 2Fe rubredoxin and the production of Cd-substituted rubredoxin suitable for structural studies by NMR (*28*). As part of our structural and kinetic work on this redox system, we now present a detailed kinetic and thermodynamic analysis of the eT reactions in the RR−rubredoxin eT complex. Our work demonstrates that both the 1Fe and 2Fe forms of rubredoxin combine with RR to form functional eT complexes and that reaction rates within each complex are comparable. Our analysis of the reaction kinetics using both transition state and eT theories also demonstrates that eT to the 1Fe and 2Fe forms of rubredoxin is gated by an adiabatic event prior to the eT step.

## EXPERIMENTAL PROCEDURES

*Chemicals and Enzymes*. Complex bacteriological media were from Unipath and all media were prepared as described by Sambrook et al. (*29*). $\beta$-NADH, xanthine, xanthine oxidase, benzyl viologen, and phenosafranin were from Sigma. Vent DNA polymerase was from New England Biolabs, and restriction enzymes and the expression plasmid pKK223-3 were from Pharmacia. Timentin was from Beecham Research Labs. All other chemicals were of analytical grade where possible. *Ps. oleovorans* rubredoxin was isolated from a recombinant strain of *Escherichia coli* as previously described (*28*). The 2Fe form was generated from the 1Fe form following denaturation with trichloroacetic acid and refolding in the presence of excess ferrous ammonium sulfate (*28*). The concentrations of each form of rubredoxin were determined at 497 nm (1Fe form) or 495 nm (2Fe form) using extinction coefficients of 6300 $M^{-1}$ $cm^{-1}$ (1Fe form) and 10 600 $M^{-1}cm^{-1}$ (2Fe form) in 50 mM potassium phosphate buffer, pH 7.0 (*17*, *28*).

*Overexpression and Purification of RR*. *Ps. oleovorans* chromosomal DNA for PCR was prepared by suspending a single colony from a plate into 0.5 mL of water. The suspension was boiled for 5 min and centrifuged to remove debris. Supernatant (5 $\mu$L) was used as template in PCR reactions using the oligonucleotides 5′-TTTTTTTTTGAATTCATGGCAATCGTTGTTGTTGGCGCT-3′ and 5′-TTTTTTTTTTAAGCTTCTAATCAGGTAATTTTATACTCCC-3′ designed from the published sequence of the gene (*alk*T) encoding RR (*30*). The amplified gene was digested with *Eco*RI and *Hin*dIII and cloned into the expression vector pKK223-3 to produce plasmid pKRR5V and sequenced. RR was purified from 10 L cultures (harvested at an optical density of ∼4 at 600 nm) of the overexpressing host (*E. coli* strain JM109) grown at 18 °C. Cells were resuspended in 100 mL of buffer A (20 mM potassium phosphate, pH 7.6, and 20% glycerol) and disrupted by passage through a French Press. The clarified extract was fractionated with ammonium sulfate, and the 30−60% saturation precipitate was retained and resuspended in buffer A. Following dialysis, the enzyme was applied to a DEAE (DE-52) ion-exchange column (3.5 × 30 cm) equilibrated in buffer A, and after washing with buffer A (2 column vol), the column was developed with a 0 to 0.1 M KCl gradient contained in buffer A. Fractions containing enzyme (>10 units/mL) were pooled, dialyzed against buffer A, and concentrated to about 30 mL by ultrafiltration and then applied to a Cibracon Blue column (2.5 × 10 cm) equilibrated with buffer A. After washing (10 column vol) with buffer A, the column was developed using a 0 to 1 M KCl gradient contained in buffer A. Fractions (>20 units/mL) were dialyzed exhaustively against 50 mM potassium phosphate, pH 7.0, and 20% glycerol (buffer B) and concentrated by ultrafiltration. The concentration of purified RR was determined using an extinction coefficient of 11 100 $M^{-1}$ $cm^{-1}$ at 450 nm (18). Glycerol (20%) is required to maintain RR activity.

*Redox Potentiometry*. Potentiometric titrations of RR were conducted using the xanthine oxidase method developed by Massey (*31*). RR was contained in 50 mM potassium phosphate buffer, pH 7.0, and 20% glycerol and made anaerobic in a sidearm cuvette along with 290 $\mu$M xanthine, 2 $\mu$M benzyl viologen, and 20 $\mu$M phenosafranin (−244 mV), in a total volume of 2 mL. Xanthine oxidase (20 $\mu$L of a 66 $\mu$M stock) was placed in the sidearm of the apparatus. After achievement of anaerobosis by repeated evacuation and flushing with oxygen-free argon, the UV−vis spectrum of the mixture was recorded using a Hewlett-Packard 8452a diode array spectrophotometer. Reduction of the dye was initiated by tipping xanthine oxidase from the sidearm into the mixture. Spectra were recorded at 10 min intervals. The extent of reduction of RR and the dye was determined from absorbance changes at 412 nm (an isosbestic for phenosafranin) and 526 nm, respectively. The midpoint potential of RR was determined from a plot of $\log[\text{phenosafranin}_{ox}]/[\text{phenosafranin}_{red}]$ against $\log[RR_{ox}]/[RR_{red}]$. The redox potential was determined at 5 °C.

*Kinetic Measurements*. Rapid reaction kinetic experiments were performed using an Applied Photophysics SX.17MV stopped-flow apparatus. Time-dependent reductions of RR with NADH were performed by multiple wavelength stopped-flow spectroscopy using a photodiode array detector and X-SCAN software (Applied Photophysics). Spectral deconvolution was performed by global analysis and numerical integration methods using PROKIN software (Applied Photophysics). For single wavelength work, data collected at 450 and 750 nm were analyzed using nonlinear least-squares

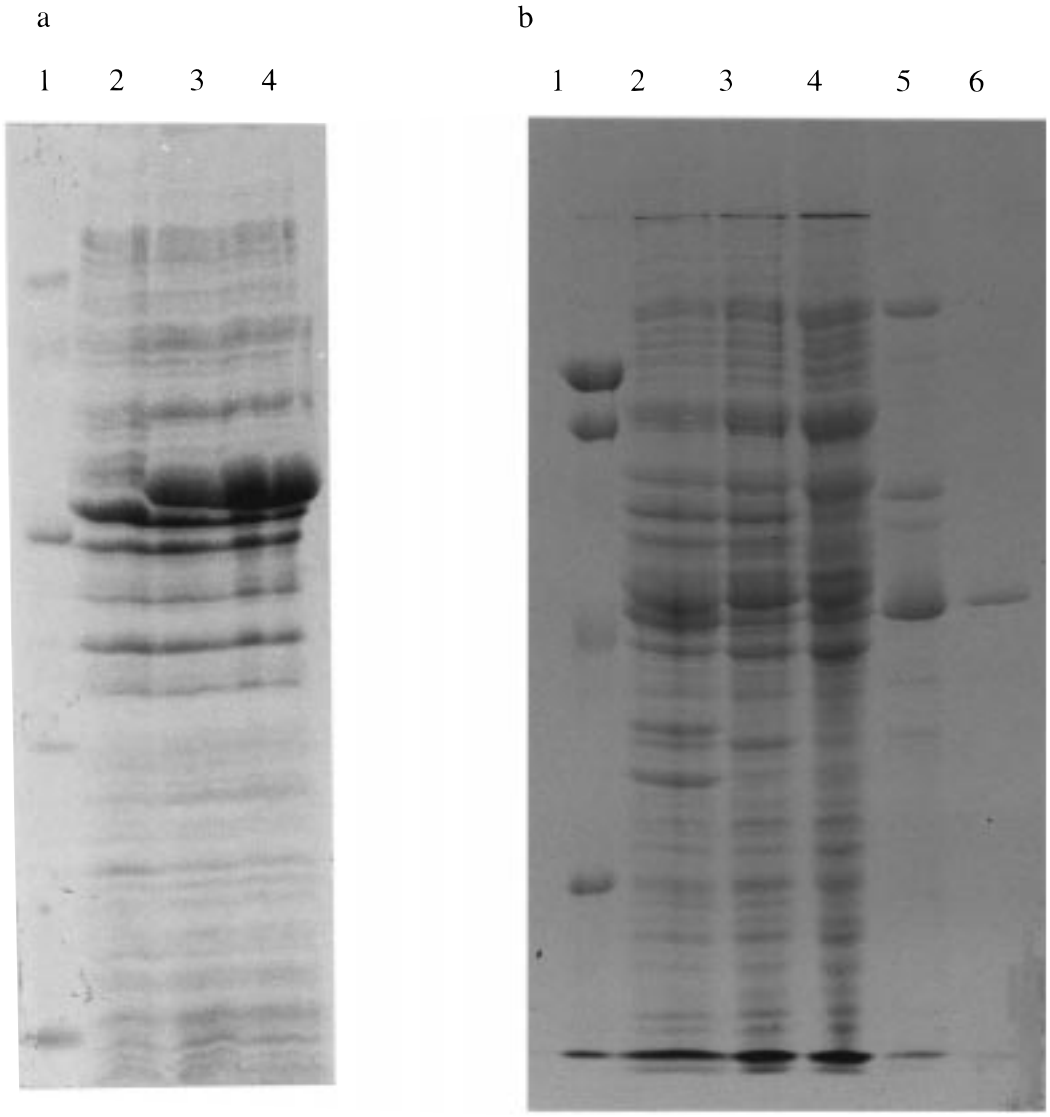


FIGURE 1: Expression of *Ps. oleovorans* RR in *E. coli* strain JM109 and analysis of samples taken at various points during the purification procedure. (a) Expression analysis by 15% SDS PAGE. Lane 1, molecular mass markers (63, 45, 29, and 14 kDa); lane 2, *E. coli* strain JM109; lane 3, *E. coli* strain JM109 transformed with plasmid pKRR5V; lane 4, *E. coli* strain JM109 transformed with plasmid pKRR5V and induced with 2 mM isopropyl $\beta$-D-thiogalactoside. (b) Analysis of the purification of RR by 10% SDS−PAGE. Lane 1, molecular mass markers (83, 63, 45, and 29 kDa); lane 2, *E. coli* strain JM109 transformed with plasmid pKRR5V; lane 3, clarified supernatant after cell breakage; lane 4, resolubilized 30−60% ammonium sulfate fraction; lane 5, eluate from DE−52 anion exchange chromatography; lane 6, eluate from cibracon Blue affinity chromatography.

regression analysis on an Archimedes 410-1 microcomputer using Spectrakinetics software (Applied Photophysics). Experiments were performed by mixing RR in the appropriate buffer with an equal volume of NADH in the same buffer at the desired concentration. For studies of the oxidative half-reaction, the sequential mixing mode of the reaction analyzer was employed. RR was rapidly mixed with a stoichiometric amount of NADH to facilitate reduction of the enzyme-bound flavin and after a suitable aging period (see below), rubredoxin was rapidly mixed with the reduced enzyme solution and reduction of rubredoxin was monitored at 540 nm. The intrinsic oxidase activities of RR and rubredoxin were found to be sufficiently slow to enable the use of sequential mixing protocols for analysis of the oxidative half-reaction. In both reductive and oxidative half-reactions, pseudo-first-order conditions were maintained by having NADH (reductive half-reaction) or rubredoxin (oxidative half-reaction) at least 10-fold in excess of RR. For each reaction, at least five replica measurements were collected and averaged.

Observed rate constants for flavin absorption changes at 450 nm (flavin reduction) in the reductive half-reaction were obtained from fits of the data to eq 1

$$A_{450} = Ce^{-k_{obs}t} + b \quad (1)$$

and observed rate constants for absorption changes at 750 nm (charge-transfer complex formation) in the reductive half-reaction were obtained from fits to eq 2

$$A_{750} = C(1 - e^{-k_{obs}t}) + b \quad (2)$$

In both eqs 1 and 2, $C$ is a constant related to the initial absorbance and $b$ is an offset value to account for a nonzero baseline. The reductive half-reaction sequence was modeled as shown in the general scheme

$$A + B \underset{k_2}{\overset{k_1}{\rightleftharpoons}} C \xrightarrow{k_3} D \quad (3)$$

where A = $RR_{ox}$, B = NADH, C = Michaelis complex, and D = is a charge-transfer intermediate of RR containing the two-electron reduced (dihydroflavin) form of the flavin and $NAD^+$. Data were fitted to eq 4 (*32*):

$$k_{obs} = \frac{k_3[S]}{K_d + [S]} \quad (4)$$

Reduction of rubredoxin by reduced RR was observed at 540 nm. Transients were found to be monophasic for both the 1Fe and 2Fe forms of rubredoxin, and observed rate constants were calculated by fitting transients to a monophasic expression. Observed rates were hyperbolically dependent on rubredoxin concentration, and values for the limiting rate constant and complex dissociation constant were calculated by fitting data to the equation described by Strickland (ref *32*; eq 4). Modeling of the reaction sequence for the oxidative half-reactions with 1Fe and 2Fe rubredoxins is discussed in more detail in Results—a conceptually similar scheme to that described for 1Fe rubredoxin has been described elsewhere (*33*). All curve fitting was performed using the Grafit software package (*34*).

## RESULTS AND DISCUSSION

*Purification and Properties of Recombinant RR.* Transformation of plasmid pKRR5V into *E. coli* strain JM109 leads to the high level expression of recombinant RR (Figure 1). However, to maximize the yield of soluble RR, cultures were grown at 18 °C, since at higher temperatures RR was found to partition into the insoluble fraction of clarified cell lysates. Enzyme was obtained in adequate yield for detailed kinetic analysis (Table 1) and as a homogeneous sample (Figure 1) using the procedure described above and displayed spectral properties (Figure 2) identical to those reported previously for RR purified from *Ps. oleovorans* (*18*). The reduction potential of recombinant RR was found to be −247 mV (Figure 3), consistent with its need to accept electrons from NADH (−320 mV) and subsequently transfer them to 1Fe [the non physiological form; −6 mV (*28*)] or 2Fe [the physiological form; −8 mV (*28*)] forms of rubredoxin. Reduction of RR in the absence of phenosafranin demonstrated that reduction was direct to the dihydroflavin form.

*Multiple and Single Wavelength Stopped-Flow Studies of the Reductive Half-Reaction.* Analysis of the spectral changes occurring during the reduction of RR with NADH were investigated using rapid-mixing photodiode array spectroscopy. Reduction of the enzyme with $\beta$-NADH at pH 7.0 with a stoichiometric concentration of coenzyme revealed that only two enzyme species were detectable. Control reactions of enzyme mixed with reaction buffer in the absence of coenzyme indicated that spectral changes did not occur within the dead time of the stopped-flow instrument (1 ms) during the reactions with NADH. Therefore, there is no evidence for a spectroscopically distinct enzyme−NADH complex prior to enzyme reduction as seen with some other flavoproteins (e.g., ref *35*), thereby confirming the validity of the reaction model used (eqs 3 and 4). Kinetic data obtained by photodiode array spectroscopy were analyzed globally by numerical integration using a two state model (A → B), where A = oxidized enzyme and B = an enzyme−coenzyme charge-transfer complex containing the two electron-reduced flavin (dihydroflavin) and $NAD^+$. Formation of the reduced enzyme−$NAD^+$ charge-transfer complex gives rise to an absorbance increase at long wavelengths (550 to >800 nm) and its formation is commensurate with flavin reduction (bleaching at 450 nm; Figure 4).

Table 1: Purification of RR from *E. coli* Strain JM109 Transformed with Plasmid pKRR5V[a]

| sample | vol (mL) | activity (units) | protein (mg) | specific activity (units/mg) | yield (%) |
|---|---|---|---|---|---|
| initial extract | 75 | 8025 | 2100 | 3.8 | 100 |
| 30−60% $(NH_4)_2SO_4$ | 26 | 3268 | 390 | 8.4 | 41 |
| DE52 | 17 | 2735 | 58 | 47.1 | 34 |
| cibracon Blue | 10 | 928 | 11 | 86 | 12 |

[a] Assay of RR was as described previously by Ueda and Coon (*18*). RR (1 unit) reduces 1 $\mu$mol of horse cytochrome *c*/min under the defined reaction conditions (*18*).

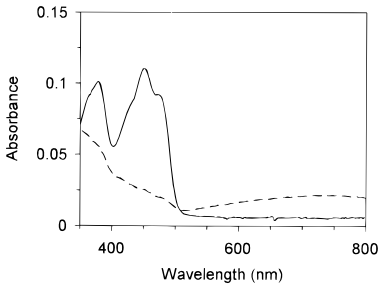


FIGURE 2: UV−vis spectra of oxidized and reduced RR. Spectra were recorded for RR (10 $\mu$M) contained in 50 mM potassium phosphate buffer, pH 7.0, and 20% glycerol under anaerobic conditions. Upper curve, spectrum of oxidized enzyme; lower curve, spectrum of RR reduced with a stoichiometric concentration of NADH illustrating bleaching of the absorbance at 450 nm and appearance of a reduced enzyme−$NAD^+$ charge-transfer complex at long wavelength.

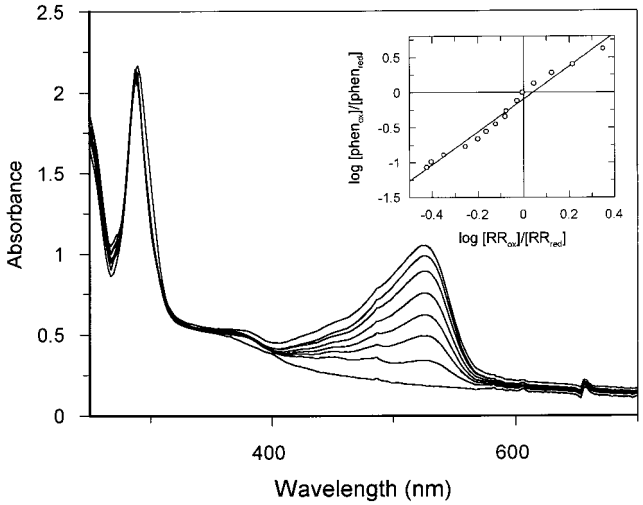


FIGURE 3: Potentiometric titration of the FAD in RR. Oxidized RR contained in 50 mM potassium phosphate buffer, pH 7.0, and 20% glycerol was mixed with phenosafranin (20 $\mu$M), xanthine (290 $\mu$M), RR (20 $\mu$M), and benzyl viologen (2 $\mu$M) under anaerobic conditions. Reduction was initiated by addition of xanthine oxidase (20 $\mu$L of a 66 $\mu$M stock) from the sidearm of the tonometer. Scans were recorded every 10 min (not all scans are shown). (Inset) Plot of log $[phenosafranin]_{ox}/[phenosafranin]_{red}$ against log $[RR]_{ox}/[RR]_{red}$. Midpoint potential is −247 mV.

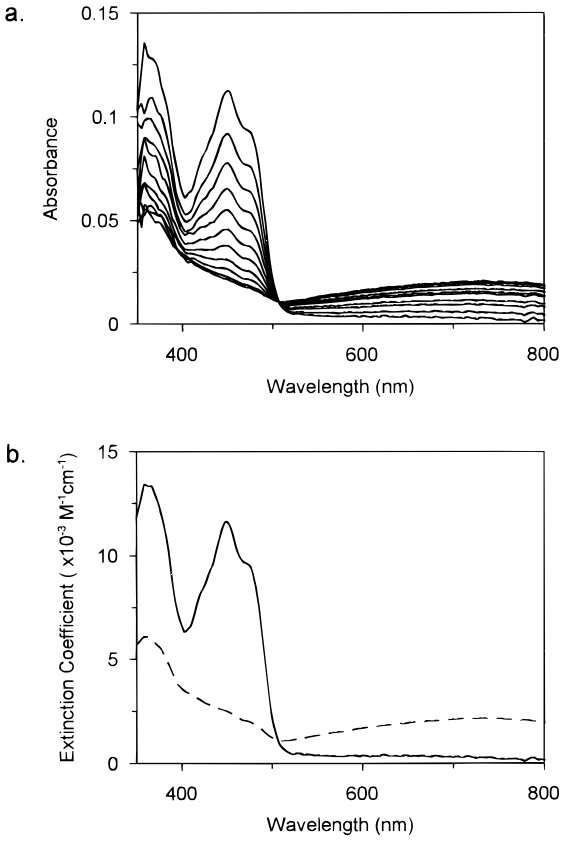


FIGURE 4: Time-dependent spectral changes for the reaction of RR with NADH at 5 °C and deconvoluted spectra of intermediates. (a) Time-dependent spectral changes. Enzyme (cell concentration 10 $\mu$M) was reduced with NADH (concentration 10 $\mu$M) in 50 mM potassium phosphate buffer, pH 7.0, and 20% glycerol. The first spectrum was recorded 1.28 ms after mixing (not all spectra are shown). (b) Deconvoluted spectra obtained by global analysis using ProKin software. Spectrum 1 (solid line), oxidized enzyme; spectrum 2 (hatched line), two electron-reduced RR−NAD$^+$ charge-transfer intermediate.

Single wavelength measurements at 450 nm (reduction of flavin) and 750 nm (charge-transfer formation) were performed to evaluate the substrate dependence of the reductive half-reaction. As observed with the photodiode array work, when stoichiometric amounts of NADH were used, RR was rapidly converted to the dihydroflavin-NAD$^+$ charge transfer form, but reoxidation by molecular oxygen was very slow and only partially complete after 500 s from the mixing event (rate constant 0.006 s$^{-1}$ at 5 °C; Figure 5c). Given the rapid reduction rates (Figure 5, panels a and b) and very slow oxidase rates, anaerobic conditions were not utilized during reductive reactions since rates could be readily analyzed without interference from flavin reoxidation. Analysis at both wavelengths revealed that the limiting rate of flavin reduction is 180 ± 4 s$^{-1}$ at 5 °C which corresponds, within error, to the limiting rate of charge-transfer formation determined at 750 nm (189 ± 7 s$^{-1}$); dissociation constants measured at both wavelengths are comparable (36 ± 2 and 43 ± 5 $\mu$M measured at 450 and 750 nm, respectively). The data serve to emphasize that flavin reduction and charge-transfer formation are equivalent kinetic steps in the reductive half-reaction.

Rate constants for flavin reduction were analyzed using the Arrhenius equation, written in terms of transition state theory (eq 5)

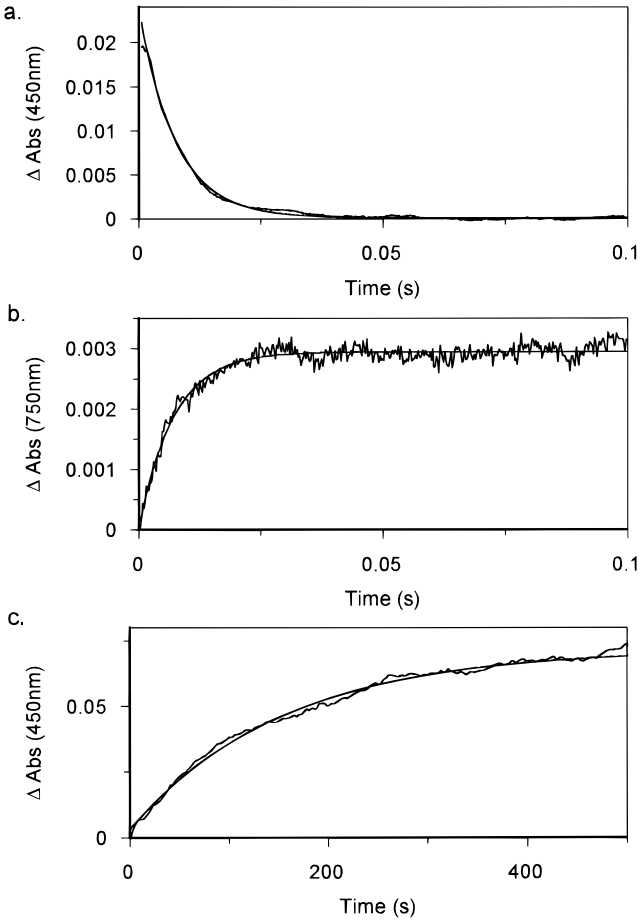


FIGURE 5: Kinetic transients observed for the reductive half-reaction of RR in 50 mM potassium phosphate buffer, pH 7.0, and 20% glycerol at 5 °C. (a) Transient observed at 450 nm. Concentration of RR and NADH is 3 and 105 $\mu$M, respectively. (b) Transient observed at 750 nm. Concentration of RR and NADH is 6 and 105 $\mu$M, respectively. (c) Transient observed at 450 nm and long time base to illustrate oxidase activity. RR and NADH concentration is 12 $\mu$M.

$$k = \frac{k_B}{h} T e^{-\Delta G^{\ddagger}/RT} = \frac{k_B}{h} T e^{-\Delta H^{\ddagger}/RT} e^{\Delta S^{\ddagger}/R} \qquad (5)$$

where $k_B$ is Boltzmann's constant and $h$ is Planck's constant. Data were fitted to eq 6, and values of $\Delta S^{\ddagger}$ and $\Delta H^{\ddagger}$ were calculated from the values of the ordinate intercept and gradient, respectively (Figure 6)

$$R\left[\ln\left(\frac{k}{T}\right) - \ln\left(\frac{k_B}{h}\right)\right] = \Delta S^{\ddagger} - \Delta H^{\ddagger}\left(\frac{1}{T}\right) \qquad (6)$$

The errors in the calculated $\Delta S^{\ddagger}$ will be larger than those for $\Delta H^{\ddagger}$ due to the large extrapolation to the ordinate axis, but the analysis is not substantially compromised; the validity of performing an extrapolation to the ordinate axis to calculate $\Delta S^{\ddagger}$ has been discussed recently (*35*). Rates of flavin reduction as a function of temperature were determined using an NADH concentration of 500 $\mu$M (i.e., approximately 13$K_d$). Analysis by eq 6 revealed a negative change in entropy ($\Delta S^{\ddagger} = -65.8 \pm 2.2$ J mol$^{-1}$ K$^{-1}$). This ordering effect may reflect charge development in the transition state—positive charge develops on the nicotinamide and negative charge in the N1/C2 carbonyl region of the flavin—leading to an ordering of water molecules in the active site, although

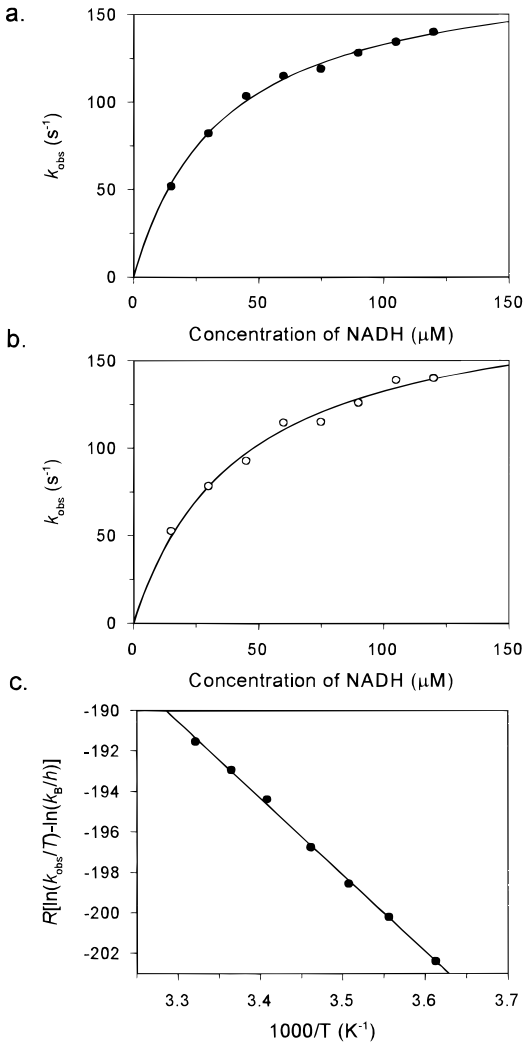


FIGURE 6: Concentration dependence of the observed rates measured at 450 nm (flavin reduction) and 750 nm (charge-transfer formation) for the reductive half-reaction of RR. (a) data for 450 nm transients; (b) data for 750 nm transients. Conditions: reactions at 450 nm, 3 $\mu$M RR, 50 mM potassium phosphate buffer, pH 7.0, and 20% glycerol, 5 °C; reactions at 750 nm, 6 $\mu$M RR, 50 mM potassium phosphate buffer, pH 7.0, and 20% glycerol, 5 °C, except for points at NADH concentrations of 15 and 30 $\mu$M where the RR concentrations were 1.5 and 3 $\mu$M, respectively. (c) Thermodynamic analysis of the kinetics of flavin reduction in the reductive half-reaction of RR. Conditions: 6 $\mu$M RR and 500 $\mu$M NADH. $\Delta S^{\ddagger} = -65.8 \pm 2.2$ J mol$^{-1}$ K$^{-1}$; $\Delta H^{\ddagger} = 37.8 \pm 0.6$ kJ mol$^{-1}$, and $\Delta G^{\ddagger}$ (at 298 K) $= 57.5 \pm 0.7$ kJ mol$^{-1}$.

this will be offset to some degree by the expulsion of water on immobilizing the coenzyme in the active site. The enthalpic contribution ($\Delta H^{\ddagger}$) to the reaction is $37.8 \pm 0.6$ kJ mol$^{-1}$ and the corresponding Gibb's free energy change ($\Delta G^{\ddagger}$) calculated at 298 K is $57.5 \pm 0.7$ kJ mol$^{-1}$.

*Complex Formation and Sequential Stopped-Flow Studies of Electron Transfer to Rubredoxin.* Analysis of the UV−vis spectrum of the eT complex with either 1Fe and 2Fe rubredoxin revealed a small but significant change in spectral signature at about 350 and 500 nm compared with the sum of the spectra for the component proteins (Figure 7). The difference spectra for both the 1Fe and 2Fe complexes were found to be similar (Figure 7), and these changes in electronic spectra may report on minor structural perturbations during complex formation and/or local environmental effects around the flavin redox center. Any small structural perturbation

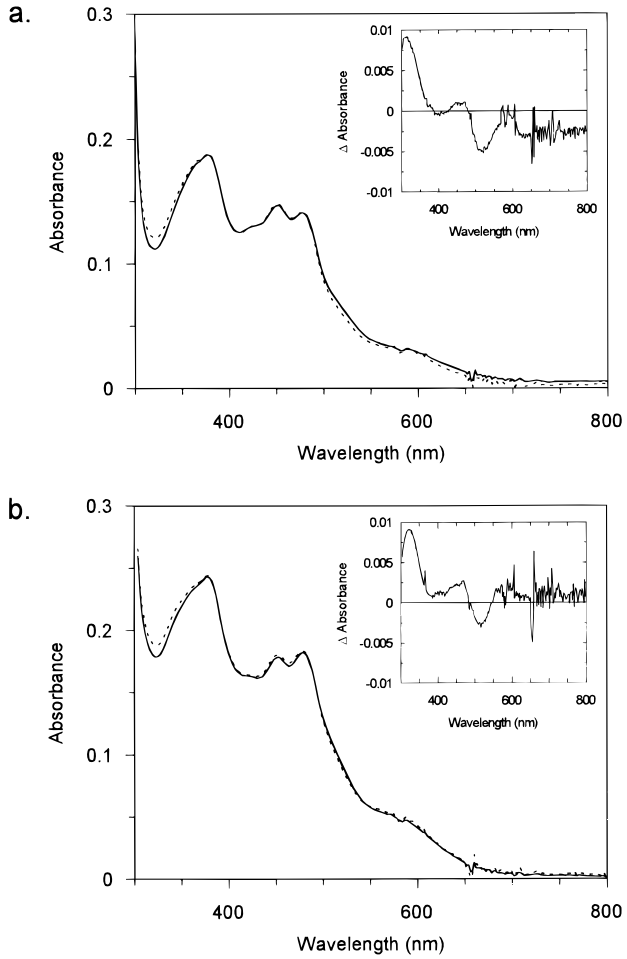


FIGURE 7: Changes in electronic spectra on formation of the RR-rubredoxin eT complex. (a) Spectral analysis of the RR−1Fe complex. Solid line, spectrum recorded for a mixture of RR and 1Fe rubredoxin in 50 mM potassium phosphate buffer, pH 7.0, and 20% glycerol (concentration of each component was 10 $\mu$M). Hatched line, sum of individual spectra for RR and 1Fe rubredoxin measured under identical conditions to that above. (Inset) difference spectrum (mixture spectrum minus individual component spectra). (b) as for panel a but using 2Fe rubredoxin in place of 1Fe rubredoxin.

may be relevant in the interpretation of the observed kinetic behavior in our studies of the oxidative half-reaction (see below). Studies of the reductive half-reaction under aerobic conditions with stoichiometric amounts of NADH indicated that the intrinsic oxidase activity of RR is slow (0.006 s$^{-1}$). The possibility of investigating eT from RR to rubredoxin under aerobic conditions using a sequential stopped-flow method was therefore explored. A procedure of this type negates the use of anaerobic conditions and the mixing of dithionite-reduced RR with rubredoxin—a technically more demanding way of studying the oxidative half-reaction. In photodiode array work with 1Fe rubredoxin, NADH (2.5 $\mu$M) and RR (5 $\mu$M) were rapidly mixed, and following an appropriate delay (5 s) to enable reduction of the enzyme, 1Fe rubredoxin (5 $\mu$M) was mixed with the aged reaction—the half stoichiometric concentration of NADH (2 electron donor) ensured that RR was fully reoxidized and 1Fe rubredoxin was fully reduced on completion of the reaction. For studies with 2Fe rubredoxin, the rubredoxin and RR concentrations were 5 $\mu$M, but the NADH concentration was increased to 5 $\mu$M—2Fe rubredoxin accepts two electrons

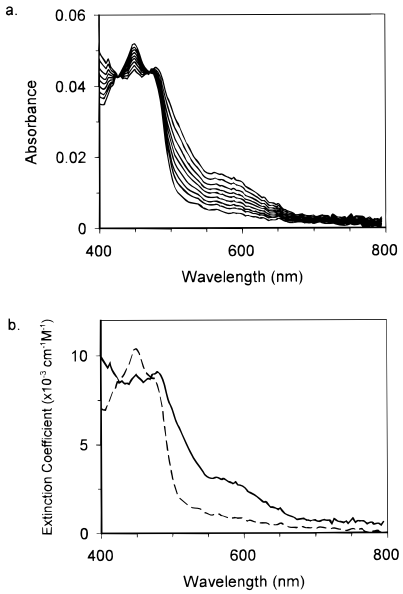


FIGURE 8: Time-dependent spectral changes for the reaction of reduced RR with 1Fe rubredoxin. (a) Spectral changes for 1Fe rubredoxin. Conditions: 2.5 $\mu$M NADH, 5 $\mu$M RR and 5 $\mu$M 1Fe rubredoxin, 50 mM potassium phosphate buffer, pH 7.0 and 20% glycerol, 5 °C. Delay time 5 s. First spectrum is recorded at 1.28 ms; not all spectra are shown. (b) deconvoluted spectra by fitting to a two-species model obtained by global analysis and numerical integration methods. Initial spectrum (solid line), final spectrum (hatched line). Similar spectral changes were seen for reactions performed with the 2Fe rubredoxin.

from RR. A sequential mixing protocol of the type described is only valid if the rate of reoxidation of reduced RR by rubredoxin is substantially faster than that by molecular oxygen. In this case, the rates of reoxidation in reactions using stoichiometric amounts of 1Fe and 2Fe rubredoxins were found to be at least 5000-fold greater than the rate of reoxidation by molecular oxygen.

The spectral changes accompanying the oxidative half-reactions of two electron-reduced RR with 1Fe and 2Fe rubredoxins at pH 7.0 were analyzed by photodiode array spectroscopy. In both cases, the reaction sequence was best described by a simple two species model (A → B) and global fitting using numerical integration methods was used to generate the initial and final spectra of the reaction mixture (Figure 8). The spectrum of species A resembles a mixture of the two electron-reduced-$NAD^+$ charge-transfer complex of RR and oxidized 1Fe or 2Fe rubredoxin. The spectrum of species B is that of oxidized RR and reduced rubredoxin. The photodiode array analyses revealed (i) 540 nm is a convenient wavelength for following the kinetics of rubredoxin reduction as there are no major spectral changes attributed to RR at this wavelength and (ii) additional, spectroscopically distinct intermediates (e.g., flavin semiquinone)—not observed in simple optical titrations, e.g., see above—do not accumulate in the oxidative half-reaction (however, flavin semiquinone formation must occur transiently during the oxidative half-reaction since eT to 1Fe rubredoxin is a 1 electron-transfer reaction). As expected for a simple two species model (A → B), photodiode array transients at 540 nm were monophasic. This finding was corroborated in single wavelength studies at 540 nm in which the quality of kinetic transients is greatly improved (Figure 9). This is a key observation for the reaction sequence modeling of the oxidative half-reaction discussed below.

The dependence of the oxidative half-reaction on rubredoxin concentration was analyzed under pseudo-first-order conditions for both the 1Fe and 2Fe forms of rubredoxin (Figure 9) at pH 7.0 and 5 °C. In both cases, a hyperbolic dependence was observed—limiting rates for rubredoxin reduction [72.7 ± 0.6 $s^{-1}$ (1Fe rubredoxin) and 55.2 ± 0.3 $s^{-1}$ (2Fe rubredoxin)] and dissociation constants for the complex [12.5 ± 0.5 $\mu$M (1Fe rubredoxin) and 4.5 ± 0.2 $\mu$M (2Fe rubredoxin)] were calculated by fitting to eq 4. The significance of the differences in the calculated kinetic parameters for 1Fe and 2Fe rubredoxins should be interpreted with caution: to maintain pseudo first-order conditions and

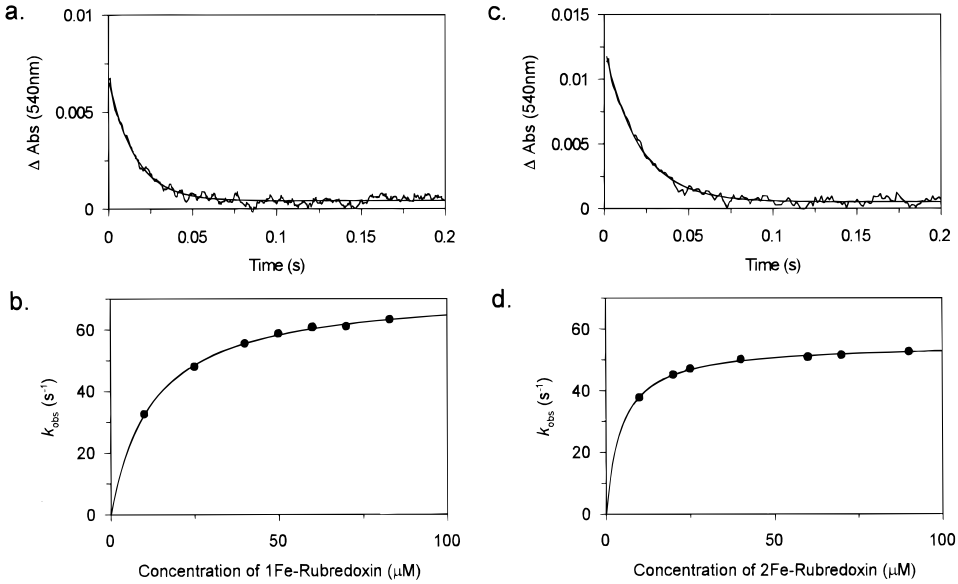


FIGURE 9: Transients observed at 540 nm and concentration dependence of the observed rates measured at 540 nm (rubredoxin reduction). (a) Transient observed at 540 nm for the 1Fe rubredoxin (83 $\mu$M). (b) Concentration dependence of the oxidative half-reaction with 1Fe rubredoxin. (c) Transient observed at 540 nm for the 2Fe rubredoxin. (d) Concentration dependence of the oxidative half-reaction with 2Fe rubredoxin (90 $\mu$M). Conditions: 50 mM potassium phosphate buffer, pH 7.0, and 20% glycerol, 5 °C. For the 1Fe rubredoxin experiments, 2.5 $\mu$M RR, and half stoichiometric NADH were used (except for the 12.5 $\mu$M rubredoxin point for which 1.25 $\mu$M RR and half stoichiometric NADH were used). For the 2Fe rubredoxin experiments, conditions were as for the 1Fe form.

a sizable spectroscopic signal, the lower limit of the rubredoxin concentrations used to calculate the kinetic parameters is greater than the value of the dissociation constant. This leads to poor definition of the curve at low rubredoxin concentrations. However, it is clear that the determined kinetic parameters for 1Fe and 2Fe rubredoxins are similar. A major question arising from this work is the precise meaning of the limiting rate for rubredoxin reduction—this aspect is discussed below.

*Reaction Sequences for the Oxidative Half-Reaction.* The simple kinetic behavior observed for the oxidative half-reaction is perhaps surprising given the complexity of this half-reaction with 1Fe and 2Fe rubredoxins. In the case of 2Fe rubredoxin, a minimal kinetic scheme involves the binding of rubredoxin to reduced RR to form an eT complex followed by the transfer of two electrons to the 2Fe atoms of rubredoxin. The lack of a lag phase in the 540 nm transients suggests the rapid equilibrium assumption on the binding step is appropriate. The sequential eT reactions can either be (i) direct from flavin to each Fe atom or (ii) to the same Fe atom in rubredoxin, thus involving an additional eT within the rubredoxin molecule itself. In both cases, the first eT reaction from RR involves a flavin dihydroquinone/semiquinone redox couple and the second eT reaction a semiquinone/oxidized flavin redox couple. Each redox couple has a unique midpoint potential which contributes to a unique rate for each eT. Thus, for an eT-limited process, biphasic transients would result if the rate of the first eT is greater than the second. Conversely, the transients would be monophasic if the rate of the first eT is slower than the second. The observed transients at 540 nm are monophasic suggesting the latter scenario. However, monophasic transients can also result if the observed rates are not *intrinsic* eT rates, but reflect a rate-limiting preceding step (e.g., a change in complex geometry) in the reaction sequence that gates the eT event.

The oxidative half-reaction with 1Fe rubredoxin is more complex than the corresponding reaction with 2Fe rubredoxin. With 1Fe rubredoxin, a minimal sequential oxidative half-reaction of the following type can be used to describe the reaction sequence:

$$RR_{red} + R_{ox} \underset{k_2}{\overset{k_1}{\rightleftharpoons}} RR_{red}R_{ox} \underset{k_4}{\overset{k_3}{\rightleftharpoons}} RR_{sq} + R_{red}$$

$$RR_{sq} + R_{ox} \underset{k_6}{\overset{k_5}{\rightleftharpoons}} RR_{sq}R_{ox} \underset{k_8}{\overset{k_7}{\rightleftharpoons}} RR_{ox} + R_{red}$$

The key difference here is the need to form two eT complexes sequentially—again with the rapid equilibrium assumption applying—to enable the transfer of both electrons in RR to two molecules of 1Fe rubredoxin. As for the 2Fe rubredoxin reactions, the photodiode array data revealed that 1Fe rubredoxin reduction is complete, indicating the lack of a reverse reaction. If the reaction rate is limited by eT, then like for 2Fe rubredoxin, monophasic transients could result if $k_3$ is smaller than $k_7$. As for 2Fe rubredoxin, a rate-limiting step prior to eT could also account for the monophasic response at 540 nm and good fits to the (A → B) model in the photodiode array work. In this latter case, the minimal scheme above would need to be expanded to account for the additional kinetic intermediate responsible for rate limitation. A means of distinguishing between a rate-limiting eT reaction and a rate-limiting step prior to eT for both the 1Fe and 2Fe rubredoxins is presented below.

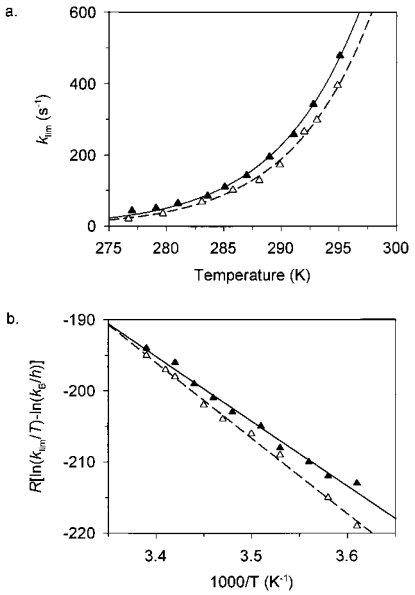


FIGURE 10: Thermodynamic analysis of the oxidative half-reaction of RR. (a) Analysis by eT theory of the 1Fe and 2Fe rubredoxin reactions, respectively. (b) Analysis by Eyring theory of the 1Fe and 2Fe rubredoxin reactions, respectively. In panel a, fits to eqs 8 and 9 are superimposable and are shown for $\Delta E_m = 200$ mV. For the 1Fe rubredoxin data fitted to eqs 8 and 9, $H_{AB} = (1.9 \times 10^6) \pm (0.9 \times 10^6)$, $\lambda = 3.8 \pm 0.14$ eV, $r = -9.8 \pm 0.6$ Å; for the 2Fe rubredoxin, $H_{AB} = (12.1 \times 10^6) \pm (1.7 \times 10^6)$, $\lambda = 4.2 \pm 0.03$ eV, $r = -12.0 \pm 1.0$ Å. In panel b, the fit is to eq 7. For the 1Fe rubredoxin, $\Delta S^{\ddagger} = 115.0 \pm 12$ J mol$^{-1}$ K$^{-1}$; $\Delta H^{\ddagger} = -91.2 \pm 3.4$ kJ mol$^{-1}$; and $\Delta G^{\ddagger}$ (at 298 K) $= -125.5 \pm 7.0$ kJ mol$^{-1}$. For the 2Fe rubredoxin, $\Delta S^{\ddagger} = 165.4 \pm 9.3$ J mol$^{-1}$ K$^{-1}$; $\Delta H^{\ddagger} = -106.3 \pm 2.7$ kJ mol$^{-1}$; and $\Delta G^{\ddagger}$ (at 298 K) $= -155.6 \pm 5.5$ kJ mol$^{-1}$.

*Temperature Dependence Studies of the Limiting Rate for Rubredoxin Reduction*. In the previous section, we advanced the hypothesis that the rate-limiting step in rubredoxin reduction might be attributed to an adiabatic event that precedes eT, rather than an eT step itself. To investigate this further, the temperature dependence of the oxidative half-reaction was studied using a rubredoxin concentration of 150 $\mu$M (essentially saturating for both the 1Fe and 2Fe eT complexes; Figure 10). Intrinsic eT reactions are nonadiabatic reactions and are best described by eT theory (*14*), whereas a rate-limiting step preceding eT would be adiabatic and best analyzed in terms of Eyring theory (i.e., eq 5). Data acquired at different temperatures were analyzed using the following equations taken from eT theory (*14*):

$$k_{ET} = \frac{4\pi^2 H_{AB}^{\ 2}}{h(4\pi\lambda RT)^{1/2}} e^{-(\Delta G^{\circ}+\lambda)^2/4\lambda RT} \quad (7)$$

$$k_{ET} = k_o e^{-\beta(r-r_o)} e^{-(\Delta G^{\circ}+\lambda)^2/4\lambda RT} \quad (8)$$

Eq 7 relates the nuclear and electronic factors to the rate of eT and consists of a classical component associated with nuclear motion and a quantum mechanical component ($H_{AB}^2$) associated with electron tunneling. $R$ is the gas constant, $h$ is Planck's constant, and $T$ is the absolute temperature. The intrinsic rate of eT is also related to distance (eq 8); in eq 8, $k_o$ is the characteristic frequency of the nuclei and is assigned a value of $10^{13}$ s$^{-1}$ (*14*, *36*) and $r_o$ represents the van der

Table 2: Physical Parameters Calculated from Temperature-Dependence Studies of the ET Reaction to Rubredoxin

| | 2Fe rubredoxin | | | 1Fe rubredoxin | | |
|---|---|---|---|---|---|---|
| $\Delta E_m$ (mV) | $H_{AB}$ ($cm^{-1} \times 10^{-6}$) | $\lambda$ (eV) | $r$ (Å) | $H_{AB}$ ($cm^{-1} \times 10^{-6}$) | $\lambda$ (eV) | $r$ (Å) |
| 50 | $6.6 \pm 0.9$ | $4.4 \pm 0.03$ | $-12.0 \pm 1.0$ | $2.8 \pm 0.7$ | $4.2 \pm 0.05$ | $-9.8 \pm 0.6$ |
| 100 | $8.2 \pm 1.2$ | $4.3 \pm 0.03$ | $-12.0 \pm 1.0$ | $2.0 \pm 0.2$ | $4.0 \pm 0.02$ | $-9.8 \pm 0.6$ |
| 150 | $10.1 \pm 3.8$ | $4.3 \pm 0.03$ | $-12.0 \pm 1.0$ | $2.0 \pm 0.2$ | $3.9 \pm 0.02$ | $-9.8 \pm 0.6$ |
| 200 | $12.1 \pm 1.7$ | $4.2 \pm 0.03$ | $-12.0 \pm 1.0$ | $1.9 \pm 0.9$ | $3.8 \pm 0.14$ | $-9.8 \pm 0.6$ |
| 300 | $6.4 \pm 0.9$ | $3.9 \pm 0.03$ | $-12.0 \pm 1.0$ | $2.8 \pm 1.1$ | $3.7 \pm 0.08$ | $-9.8 \pm 0.6$ |
| 400 | $8.1 \pm 1.1$ | $3.7 \pm 0.03$ | $-12.0 \pm 1.0$ | $2.9 \pm 0.8$ | $3.5 \pm 0.05$ | $-9.8 \pm 0.6$ |
| 500 | $6.2 \pm 0.9$ | $3.4 \pm 0.03$ | $-12.0 \pm 1.0$ | $2.7 \pm 1.1$ | $3.2 \pm 0.09$ | $-9.8 \pm 0.6$ |

Waals distance (3 Å). The electronic decay factor, $\beta$, is a coefficient that relates the decay of the electronic coupling matrix element as a function of distance; the precise value of this parameter depends on the properties of the protein bridge between redox centers, but is often approximated as 1.4 $Å^{-1}$ (*37*)—a value intermediate of that for covalently linked pathways ($\beta = 0.7$ $Å^{-1}$) and for pathways that pass through vacuum ($\beta = 2.8$ $Å^{-1}$). Semiclassical theory treats eT reactions as nonadiabatic events, and in these cases, eqs 7 and 8 apply. However, for adiabatic reactions $H_{AB}$ is large as the probability of transfer from the transition state to the product side of the energy barrier approaches unity. In these cases, the value of $H_{AB}$ is above the threshold [80 $cm^{-1}$; calculated when solvent reorganization becomes rate limiting (*38*)] for nonadiabatic reactions.

Analysis of the kinetic data is complicated by the fact that two electrons are transferred from RR to either (i) one molecule of 2Fe rubredoxin or (ii) two molecules of 1Fe rubredoxin in the oxidative half-reaction. If the limiting rates are intrinsic eT rates, then the data should be described adequately by eT theory. Fitting to eqs 7 and 8 would normally require knowledge of the driving force for the reaction, determined from a knowledge of the reduction potential of the relevant redox couple. Although the midpoint potentials of both rubredoxins are known, corresponding information for the dihydroflavin/semiquinone and semiquinone/oxidized flavin couples of RR is lacking. This arises because of the inability to populate the semiquinone form [e.g., during photoreduction (*18*)] under equilibrium conditions during potentiometric titration. Therefore, for illustrative purposes we have chosen to fit the data to eqs 7 and 8 using a range of driving forces: this range is expected to accommodate the actual values for the dihydroflavin/semiquinone and semiquinone/oxidized flavin couples of RR (Table 2). The observed rates for rubredoxin reduction (if intrinsic eT rates) will either be a limiting rate for the first or the second eT. Naturally, if the two rates are similar, the limiting rate will report on both these events, but deviation from a monophasic response is expected in this case. Since our analysis does not make use of a measured driving force for the dihydroflavin/semiquinone or the semiquinone/oxidized flavin couples of RR (instead it uses a range of driving forces that should span each of the redox couples), it is not necessary to define which eT step is being analyzed. The purpose of the analysis is to illustrate that the limiting rates for rubredoxin reduction report on either an adiabatic or nonadiabatic reaction.

Analysis of the temperature-dependent kinetic data using eqs 7 and 8 (Figure 10) yielded values for $H_{AB} \gg 80$ $cm^{-1}$ (Table 2) revealing an adiabatic reaction. Corresponding values for $\lambda$ and $r$ (Table 2) also indicated the reactions are adiabatic and thus cannot be described by eT theory. A potential complication with this analysis is that changes in protein conformation—as a result of increasing temperature—may affect redox potential. The reorganizational energies for most physiological eT reactions fall within the range ~0.7 to ~2.3 eV. These values are generally larger than the corresponding driving forces for biological eT reactions and therefore eT usually occurs within the normal region of the Marcus energy gap law (i.e., the low driving force regime $\Delta G° < \lambda$). Under these conditions, any changes in $\Delta G°$ would have to be substantial to compromise the analysis, and the likelihood of significant changes in driving force over the temperature range used is very small.

By necessity, our calculations have some in-built approximations, but the analysis clearly indicates that the measured reaction rates are not intrinsic eT rates. eT is therefore gated by some adiabatic event that precedes the eT step. In this situation, the temperature dependence of the reaction rate is best analyzed using Eyring theory (eq 6). Analysis of the data using eq 6 produced values for $\Delta S^‡$, $\Delta H^‡$, and $\Delta G^‡$ (calculated at 298 K) of $115.0 \pm 12$ J $mol^{-1}$ $K^{-1}$, $-91.2 \pm 3.4$ kJ $mol^{-1}$, and $-125.5 \pm 7.0$ kJ $mol^{-1}$ for the 1Fe rubredoxin−RR complex and $165.4 \pm 9.3$ J $mol^{-1}$ $K^{-1}$, $-106.3 \pm 2.7$ kJ $mol^{-1}$, and $-155.6 \pm 5.5$ kJ $mol^{-1}$ for the 2Fe rubredoxin−RR complex (Figure 10), respectively. The nature of the adiabatic reaction that controls eT remains to be established: possibilites include (i) configurational gating of the complex to provide the optimum geometry for eT—as suggested by the optical titration studies described above,[2] (ii) release of $NAD^+$ from the active site of reduced RR (i.e., charge-transfer decay), or (iii) reversible protonation steps (e.g., at the flavin). By using the physiological reductant (NADH) in our work rather than an artificial reductant (e.g., dithionite), it is clear that attenuation of eT by this adiabatic event is physiologically relevant.

## CONCLUSIONS

We have demonstrated that the reductive half-reaction of RR occurs by a simple one-step mechanism in which oxidized enzyme is reduced to an enzyme−$NAD^+$ charge-transfer species. The reoxidation of RR by the 1Fe (nonphysiological) and 2Fe (physiological) forms of rubredoxin is similar in kinetic terms. The data suggest that the Fe-

[2] The inclusion of 20% glycerol in all buffers may contribute to a rate-limiting adiabatic reaction that involves a conformational change. The optical titrations using RR and rubredoxin suggest structural changes may occur during complex assembly and the presence of glycerol may slow the rate of the conjectured conformational change, thus giving rise to a rate-limiting adiabatic event in the oxidative half-reaction.

containing N-terminal domain of 2Fe rubredoxin plays little or no part in complex assembly even though the N-terminal domain is reduced—directly or by rapid eT from the C-terminal Fe-domain—by RR. We have demonstrated that transfer of electrons in the assembled complex is gated by a step that precedes eT and that this adiabatic reaction is rate-limiting for eT from NADH to rubredoxin. Identifying the nature of this adiabatic reaction and elucidating the role of each iron-binding domain during eT to the $\omega$-hydroxylase are now the focus of future work.

## REFERENCES


1. Wilson, E. K., Huang, L., Sutcliffe, M. J., Mathews, F. S., Hille, R., and Scrutton, N. S. (1997) *Biochemistry 36*, 41−48.
2. Brooks, H. B., and Davidson, V. L. (1994) *Biochemistry 33*, 5696−5701.
3. Davidson, V. L., Jones, L. H., Graichen, M. E., Mathews, F. S., and Hosler, J. P. (1997) *Biochemistry 36*, 12733−12738.
4. Davidson, V. L., and Jones, L. H. (1996) *Biochemistry 35*, 8120−8125.
5. Harris, T. K., Davidson, V. L., Chen, L., Mathews, F. S., and Xia, Z.-X. (1994) *Biochemistry 33*, 12600−12608.
6. Qin, L., and Kostic, N. M. (1993) *Biochemistry 32*, 6073−6080.
7. Chen, L., Durley, R. C. E., Mathews, F. S., and Davidson, V. L. (1994) *Science 264*, 86−90.
8. Merli, A., Brodersen, D. E., Morini, B., Chen, Z.-W., Durley, R. C. E., Mathews, F. S., Davidson, V. L., and Rossi, G. L. (1996) *J. Biol. Chem. 271*, 9177−9180.
9. Northrup, S. H. (1996) in *Protein Electron Transfer* (Bendall, D. S., Ed.) pp 69−98, Bios Scientific Publishers, Oxford.
10. Qin, L., and Kostic, N. M. (1994) *Biochemistry 33*, 12592−12599.
11. Bishop, G. R., and Davidson, V. L. (1995) *Biochemistry 34*, 12082−12086.
12. Bishop, G. R., and Davidson, V. L. (1997) *Biochemistry 36*, 13586−13592.
13. Chohan, K. K., Scrutton, N. S., and Sutcliffe, M. J. (1998) *Protein Pept. Lett*. (in press).
14. Marcus, R. A., and Sutin, N. (1985) *Biochim. Biophys. Acta 811*, 265−311.
15. Davidson, V. L. (1996) *Biochemistry 35*, 14035−14039.
16. Peterson, J. A., Basu, D., and Coon, M. J. (1966) *J. Biol. Chem. 241*, 5162−5164.
17. Lode, E. T., and Coon, M. J. (1971) *J. Biol. Chem. 246*, 791−802.
18. Ueda, T., and Coon, M. J. (1972) *J. Biol. Chem. 247*, 5010−5016.
19. May, S. W., and Katapodis, A. G. (1990) *Methods. Enzymol. 188*, 3−9.
20. Shanklin, J., Achim, C., Schmidt, H., Fox, B. G., and Munck, E. (1997) *Proc. Natl. Acad. Sci. U.S.A. 94*, 2981−2986.
21. Pikus, J. D., Studts, J. M., Achim, C., Kaufmann, K. E., Munck, E., Steffan, R. J., McClay, K., and Fox, B. G. (1996) *Biochemistry 35*, 9106−9119.
22. Rosenzweig, A. C., Nordlund, P., Takahara, P. M., Frederick, C. A., and Lippard, S. J. (1995) *Chem. Biol. 2*, 409−418.
23. Fox, B. G., Shanklin, J., Somerville, C., and Eckard, M. (1993) *Proc. Natl. Acad. Sci. U.S.A. 90*, 2486−2490.
24. Gupta, N., Bonomi, F., Kurtz, D. M., Ravi, N., Wang, D. L., and Huynh, B. H. (1995) *Biochemistry 34*, 3310−3318.
25. Nordlund, P., and Eklund, H. (1993) *J. Mol. Biol. 232*, 123−164.
26. Kok, M., Oldenhuis, R., van der Linden, M. P. G., Raatjes, P., Kingma, J., van Lelyveld, P. H., and Witholt, B. (1989) *J. Biol. Chem. 264*, 5435−5441.
27. McKenna, E. J., and Coon, M. J. (1970) *J. Biol. Chem. 245*, 3882−3889.
28. Lee, H. J., Lian, L.-Y., and Scrutton, N. S. (1997) *Biochem. J. 328*, 131−136.
29. Sambrook, J., Fritsch, E. F., and Maniatis, T. (1989) *Molecular Cloning: A Laboratory Manual*, 2nd ed., Cold Spring Harbor Laboratory Press, Plainview, NY.
30. Eggink, G., Engel, H., Vriend, G., Terpstra, P., and Witholt, B. (1990) *J. Mol. Biol. 212*, 135−142.
31. Massey, V. (1990) in *Flavins and Flavoproteins* (Curti, B., Ronchi, S., and Zanetti, S., Eds), pp 59−66, Walter de Gruyter, Berlin.
32. Strickland, S., Palmer, G., and Massey, V. (1975) *J. Biol. Chem. 250*, 4048−4052.
33. Wilson, E. K., Mathews, F. S., Packman, L. C., and Scrutton, N. S. (1995) *Biochemistry 34*, 2584−2591.
34. Leatherbarrow, R. J. (1990) Grafit version 2.0, Erithacus Software Ltd., Staines, U.K.
35. Craig, D. H., Moody, P. C. E., Bruce, N. C., and Scrutton, N. S. (1998) *Biochemistry 37*, 7598−7607.
36. Rees, D. C., and Farrelly, D. (1990) *The Enzymes*, Vol. 19, pp 37−96, Academic Press, Inc., New York.
37. Moser, C. C., Keske, J. M., Warncke, K., Farid, R. S., and Dutton, P. L. (1992) *Nature 355*, 796−802.
38. Gray, H. B., and Winkler, J. R. (1996) *Annu. Rev. Biochem. 65*, 537−561.


BI981853V